

Hyperspectral Data Characterization for Object Detection Applications¹

J. Kerekes, C. Siracusa, S. Orloff, D. Manolakis, G. Shaw
MIT Lincoln Laboratory
244 Wood St., Lexington, MA 02420
(781) 981-0805, (781) 981-7271 (fax), kerekes@ll.mit.edu

L. Biehl
Purdue University
West Lafayette, IN 47097

ABSTRACT

Hyperspectral imaging (HSI) electro-optical sensors, with their hundreds of contiguous spectral bands, are a rich data source useful in a variety of applications. Numerous examples have demonstrated their potential. Understanding the characteristics of HSI data is important not only for algorithm design and assessment, but also for accurate modeling in a performance prediction context. Initial results are presented from an investigation exploring the applicability of characterizing the data with the first and second spectral statistical moments.

I. INTRODUCTION

Hyperspectral data have been successfully exploited in many applications including material identification, sub-pixel object detection, and enhanced scene classification. These applications have been demonstrated through the use of traditional spectroscopic, signal processing and pattern recognition techniques. Each of these techniques makes assumptions about the characteristics (or statistics) of the data, which may or may not be appropriate, since the algorithms were originally developed for other data types. An accurate understanding of the characteristics of hyperspectral data can lead to improved algorithms.

An understanding of the data statistics is also important for developing performance assessment theory. Lincoln Laboratory has been developing a model for assessment of the end-to-end performance of hyperspectral imaging systems [1]. This model, analytical by nature, makes assumptions regarding the statistical distributions of data. In particular, the model assumes that surface material classes can be described by their first- and second-order spectral statistics and that, after application of a matched filter vector, the resulting test statistic can be modeled as a sample from a univariate Gaussian distribution on a class-by-class basis. This study was initiated to investigate the appropriateness of these model assumptions. This paper presents the methodology, results, sensitivities, and issues associated with characterizing hyperspectral data using the first- and second-order spectral moments in the context of object detection with matched filters.

II. DATA SET DESCRIPTION

The hyperspectral data used in this study were collected by the airborne HYDICE sensor [2]. HYDICE collects data with a spatial resolution of ~1 meter in 210 spectral bands covering 0.4 to 2.5 μm . The image (320 columns by 1280 rows) examined in this study was collected over a forested area at the U.S. Army Aberdeen Proving Ground.

III. CHARACTERIZATION APPROACH

In support of our model development, we have chosen to investigate the characteristics of the data primarily through analysis of the output of a matched filter detector, with a goal of determining how well the output can be approximated as a sum of Gaussians. We first perform an initial scene classification to obtain relatively homogeneous surface classes, taking care to ensure the classes are unimodal. We then consider the classes pairwise (i.e., background and object, or target, classes) and examine the output from matched filter detector. We then evaluate the differences in detection vs. false alarm curves between data-derived empirical results, and results obtained using the assumed distributions.

IV. INITIAL SCENE CLASSIFICATION

The goal of the initial scene classification was to obtain relatively homogenous classes that are spectrally unimodal and spatially consistent. Many classification approaches exist to accomplish this. We chose a step-by-step procedure which assigns every pixel in the image to one of a small number of background classes, or if failing a number of threshold tests, to an unlabelled class. The following generally describes the selected approach. Fig. 1a shows the result of this initial classification.

- Step 1) Reduce the dimensionality of the data by selecting every 5th band to simplify computations.
- Step 2) Perform a supervised Maximum Likelihood classification using a threshold on the likelihood function to define unlabelled samples.
- Step 3) Refine the result through local spatial tests and iterating using updated class statistics.

¹ This work was sponsored by the Department of the Air Force under Contract F19628-95-C-0002. Opinions, interpretations, conclusions, and recommendations are those of the author and are not necessarily endorsed by the United States Air Force.

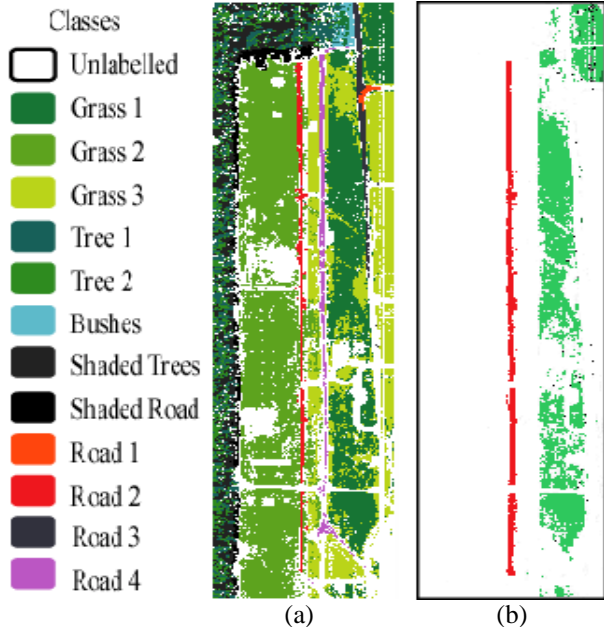


Fig. 1. a) Initial classification. b) Road 2 and Grass 1 classes used in study including pixels eliminated (black dots) from Grass 1 by editing described in Section VI.

As can be seen, the classification resulted in several subclasses for the nominal background classes of grass, tree, and road. This points to the issue of how precise one needs to define a class in order to obtain homogeneous unimodal classes. An analyst may combine all those subclasses together, but in this example the algorithm determined there was enough spectral separability to break them out as unique classes. Also, one can see many pixels that are blank, or unlabelled, which indicates they failed the threshold tests for being combined with the existing classes. These unlabelled samples most likely came from man-made objects, sensor artifacts, or perhaps were part of a background class that was not defined. In heterogeneous scenes like this, it is clear that the high-dimensionality of HSI data can lead to many classes.

V. DATA CHARACTERISTICS

In subsequent sections, we focus much of our analysis on two classes from the scene: Grass 1 and Road 2. They were chosen because of their large sample sizes (57,274 for Grass 1 and 8,049 for Road 2) and because it appeared they were not spatially contiguous, so it was less likely there would be mixed pixels consisting of samples from these two classes. Fig. 2 shows two examples of single band histograms for the Road 2 class. Overlaid on the histogram is a Gaussian curve with the same mean and standard deviation as the data.

Fig. 2a shows an example band where the Gaussian approximation is very good. Fig. 2b shows an example

where the match is much less apparent. These two examples are typical of the single band histograms for all of the classes and demonstrate that, even for the scalar marginal distributions, the data should not be considered strictly Gaussian, although in some cases it may approach Gaussian.

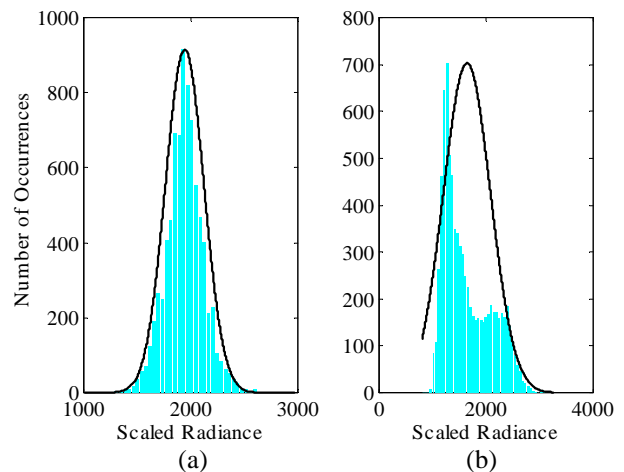


Fig. 2. Histograms for Road 2 class. Band a) 32; b) 58.

VI. DETECTION TEST STATISTIC DISTRIBUTION

In support of our primary interest in developing theory for end-to-end performance modeling, we investigated the effect of applying a normalized classical spectral matched filter to the data and examined the distributions of the 1-dimensional result. Defining the spectral mean vector and covariance matrix of the background class as m_B and Σ_B , and those for the target class as m_T and Σ_T , we examine the histograms of the output test statistic θ formed by applying the following filter w to the data samples x_n . Note that the means and covariances were estimated from the data.

$$w = \frac{\Sigma_B^{-1}(m_T - m_B)}{(m_T - m_B)^T \Sigma_B^{-1}(m_T - m_B)} \quad (1)$$

$$\theta_n = w^T (x_n - m_B) \quad (2)$$

The filter was applied to all samples from the Grass 1 and Road 2 classes where the Grass 1 class was defined to be the background and the Road 2 was defined to be the target object. Fig. 3 shows the resulting histograms for the test statistic θ calculated separately for background and target pixels. As in Fig. 2, a Gaussian curve with the same mean and standard deviation is overlaid for comparison. All results were obtained using only 145 of the 210 spectral channels as those with low signal due to atmospheric absorption were not included.

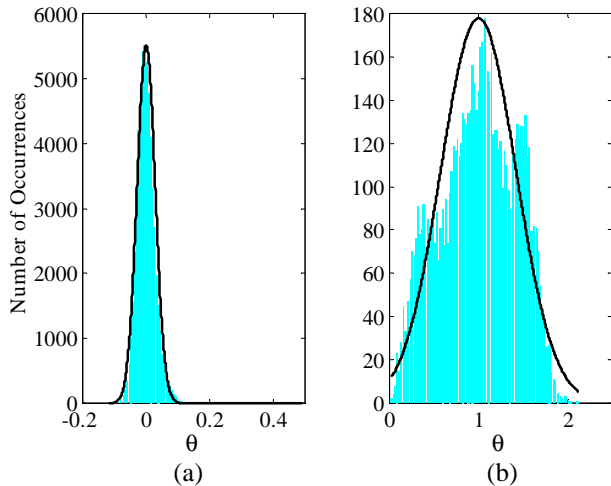


Fig. 3. Histograms of the matched filter output test statistic θ for: a) background pixels; b) target pixels.

As can be seen, the test statistic appears to be more Gaussian than the single band examples, but there are still differences, particularly for the target class. The right-hand tail of the distribution of the background class is of particular interest because those data are the source of false alarms in the object detection application. To examine the detail of the tails shown in Fig. 3a, we replot the background data with “+” symbols in Fig. 4a as cumulative distribution functions, or Q-Q plots. A straight line is shown as a reference for perfectly Gaussian data. Here, the divergence from the Gaussian curve is more obvious, particularly in the right-hand tail of the distribution.

To better understand the source of these pixels in the far right-hand tail of the Grass 1 histogram shown in Fig. 3a, we identified 237 pixels that had $\theta > 0.1$ and overlaid their location on the image shown in Figure 1b as black dots. It can be seen that many of these pixels are on the edge of the class or appear in a straight line on the image. Since HYDICE is a pushbroom sensor, this type of straight-line artifact can be attributed to bad pixel interpolation. Indeed, these particular pixels are known to have channels replaced in the data by interpolation with neighboring pixels. Figure 4b shows the resulting Q-Q plot when these pixels are removed from the background population. (The matched filter was recalculated from the edited population.) The test statistic for the background class now appears to be better modeled by a Gaussian (normal) approximation, even in the tail.

VII. RECEIVER OPERATING CHARACTERISTICS

As indicated earlier, we are most interested in understanding how the differences between the empirical analyses and analytical approximations affect the application performance prediction.

The quantitative metric selected for this evaluation is known as the Receiver Operating Characteristic (ROC). This is a curve of detection probability (P_D) vs. false alarm rate (P_{FA}). It is evaluated empirically by varying a threshold across the range of the filter vector output θ and counting the number of detections and false alarms and dividing by the total number of samples for the target and background classes, respectively. The analytical approximation to the distribution of θ based on the data mean and covariance can be characterized by the mean (3) (4) and variance (5) (6) of θ . These can be used to analytically compute P_D/P_{FA} by assuming the test statistic is Gaussian.

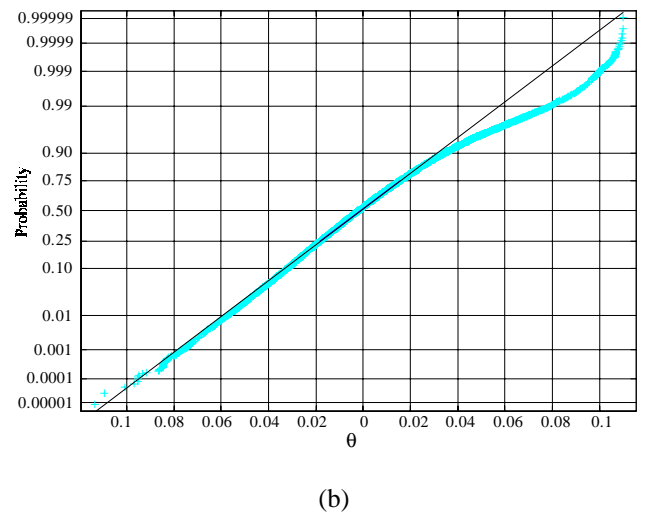
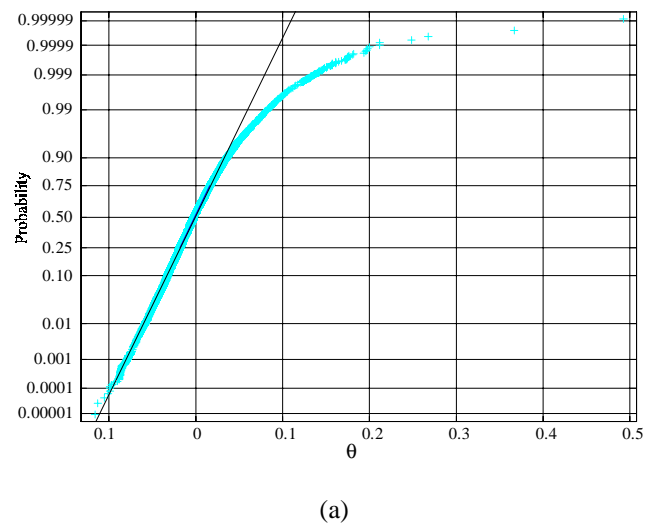


Fig. 4. Q-Q plots comparing the empirical test statistic distributions for Grass 1 pixels (+ symbols) and Gaussian data (black line) for: a) initial 57,274 pixels; and b) edited 57,037 pixels.

$$\bar{\theta}_B = 0 \quad (3)$$

$$\bar{\theta}_T = w^T (m_T - m_B) \quad (4)$$

$$\sigma_{\theta_B}^2 = w^T \Sigma_B w \quad (5)$$

$$\sigma_{\theta_T}^2 = w^T \Sigma_T w \quad (6)$$

Fig. 5 shows the comparison between: 1) the analytical approximation based only on the first- and second-order statistics, 2) the empirical curves derived from the image data, and 3) empirical curves using simulated multivariate normal (MVN) data for the target class with identical mean and covariance as the image data. There are two sets of curves. The thin curves were obtained using all 57,274 Grass 1 samples as the background, while the thick curves were obtained after editing the 237 pixels from the Grass 1 background as described earlier.

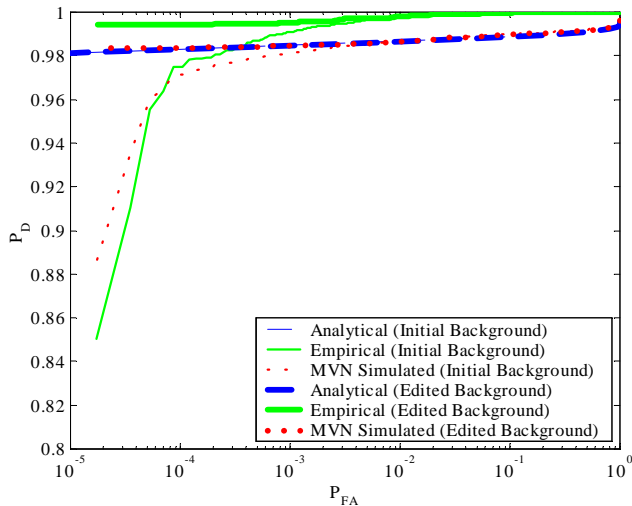


Fig. 5. P_D/P_{FA} curves comparing results from the analytical approximation, empirical, and simulated MVN data with Grass 1 as the background and Road 2 as the target, with the all initial background pixels and with the edited set.

Fig. 6 shows the same comparisons, but with a sub-pixel target simulated by taking randomly selected pairs of Road 2 vectors (weighted by 0.15) and Grass 1 vectors (weighted by 0.85) and adding them to create a sub-pixel target data set. This situation is of interest in potential road mapping applications using hyperspectral data with coarse resolution, as will be the case with the upcoming EO-1 Hyperion sensor [3] with 30 m resolution.

VIII. DISCUSSION AND CONCLUSIONS

The comparisons shown in Fig. 5 and Fig. 6 show relatively large differences in P_D for a given P_{FA} between the analytic approximations and the empirical analysis for the initial background data, but these differences are much reduced for the case with the edited background. Also,

the result obtained using MVN simulated target data shows a strikingly close comparison to the result obtained using real target data, implying that from a P_D/P_{FA} perspective, these data can be modeled as multivariate Gaussian. More to our point, we have shown that by taking care in defining the background class, one can demonstrate that the filter vector test statistic θ can be accurately modeled as Gaussian, even down to one or two false alarms (i.e., the tails of the distribution). The rationale for taking care in defining the background class seems reasonable given the occurrence of mixed pixels and sensor artifacts.

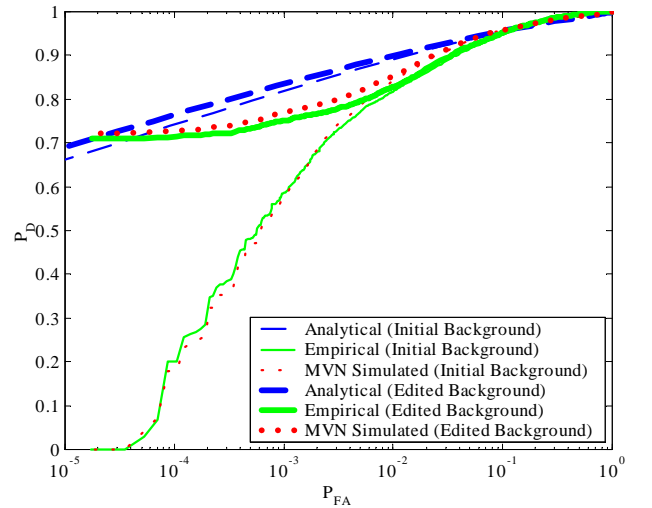


Fig. 6. P_D/P_{FA} curves comparing the empirical result with Gaussian for the case where the target is 15% Road 2 and 85% Grass 1 background.

IX. FUTURE WORK

The effort to date has focused on analyzing target detection performance with a single background. The next step will be to investigate how well the entire image can be modeled as a mixture of backgrounds. Our initial hypothesis will be that the test statistic distributions can be modeled as multiple Gaussians with means and variances calculated using only the class spectral means and covariances. However, we will also consider the applicability of other distributions as indicated by the characteristics of the data.

X. REFERENCES

- [1] J. Kerekes, J. Baum, and K. Farrar, "Analytical model of hyperspectral system performance," SPIE Vol. 3701, 1999.
- [2] L. Rickard, R. Basedow, E. Zalewski, P. Silvergate, and M. Landers, "HYDICE: An airborne system for hyperspectral imaging," SPIE Vol. 1937, 1993.
- [3] <http://eo1.gsfc.nasa.gov>.